

MEASUREMENT OF PARTICULATE SIZE  
IN SOLID PROPELLANT ROCKET MOTORS (U)\*

S. Orguc, T. E. Pruitt, T. D. Edwards, E. D. Youngborg, J. P. Powers, and D. W. Netzer  
Naval Postgraduate School  
Monterey, California 93943-5000

ABSTRACT

Small, windowed solid propellant rocket motors were used to measure the particulate sizes produced by the combustion process. Both measurements of diffractively scattered light and holography were used in the motor cavity and the former was also used in the nozzle exhaust. Automatic data retrieval of particle size data from the reconstructed holograms has also been accomplished. Progress on the particle sizing techniques and data retrieval are presented.

INTRODUCTION

Aluminum is added to solid propellants to increase performance and to suppress high frequency combustion instabilities. A small amount of a variety of additives in addition to aluminum (aluminum oxide, zirconium, etc.) are also used in reduced-smoke propellants for acoustic stabilization. In addition, there is renewed interest in dense additives ( $Hf_2O_3$ , etc.) in order to provide higher performance with low hazards propellants. Although the delivered specific impulse of metallized propellants is higher than that of the base propellants, the specific impulse efficiency is generally lower. This results from the presence of condensed metal oxides in the nozzle flow and from unburned metal within the motor port. Some particles, upon reaching the burning surface, depart immediately while others agglomerate on the surface before passing into the gas flow. Most of the metal combustion is thought to occur in the gas phase, resulting in small (typically less than two microns) metallic oxide particles. These particles are of major significance in determining the exhaust signature. In addition, particle burnout can also result in the break-up of a metallic oxide cap or layer. This can result in larger (greater than five microns) particles. The larger particles are more important in the determination of two-phase flow losses in the exhaust nozzle flow since they can lag the gas flow and, in principle, could be affected through propellant changes. There are several rather complex computer codes [Ref. 1] which attempt to model the important processes of momentum and thermal energy exchange between the solid, liquid, and gaseous phases as well as particle collisions, break-up, and wall collisions. However, these models remain semi-empirical and are generally based upon particle size distributions which were obtained from collected nozzle exhaust flows [(Ref. 2)]. Particle histories from the surface of the propellant to the nozzle exit remain largely unknown, due to the difficulty of making direct measurements within the motor and nozzle. Prediction of performance losses due to the presence of the original metal and the metal oxides are very sensitive to the assumed particle size distribution, and essentially no data are available that give this distribution as a function of position throughout the motor and nozzle.

Collecting exhaust products has been feasible only for small rocket motors. Even then, the techniques employed result in considerable variation in the measured sizes [Ref. 2]. Dobbins [Ref. 3] and Dobbins and Strand [Ref. 4] attempted to use an optical technique for measuring exhaust particle size and to compare the measurements with tank collected exhaust results. The optical technique used was a three-wavelength transmission measurement. This technique requires knowledge of particle index of refraction and the standard deviation of the particle size distribution. The optical measurements generally yielded sizes which were too small and the results were inconsistent with the collected exhaust data. It was speculated that this discrepancy resulted from a bi-model exhaust particle distribution.

Light transmission measurements have the advantage of being applicable to dense concentrations where multiple scattering occurs [Ref. 5]. However, the method works best for small particles (on the order of the wavelength of the illumination source) and requires a-priori knowledge of the particle characteristics.

Light scattering measurements can also be used to determine particle size [Refs. 6-15]. If the scattering angles used are specifically selected, the technique can be used to look almost entirely at one lobe of a bi-model size distribution. Ratioing intensities obtained at two forward scattering angles can be used to further reduce the complexity of the method. However, scattering techniques are generally thought to be applicable only to systems where the transmittance is greater than approximately 90% in order to satisfy single scattering requirements.

A combination of light transmission and light scattering measurements [Ref. 13] appears to be well-suited for many solid propellant rocket motor exhaust flows. However, experimental efforts are first needed to determine under what conditions (metal loadings, operating pressures, propellant ingredients, etc.) light scattering measurements can be made in this difficult environment.

This work was performed under F0464-87-X-0040, Air Force Astronautics Laboratory, Edwards AFB, CA.

\*Approved for public release: distribution unlimited.

The goal of the investigation to date has been to develop and compare experimental techniques that can be used for obtaining quantitative data on the effects of propellant properties, operating pressure, and nozzle geometry on the behavior of metallized particulates within the grain port and nozzle of solid propellant rocket motors. These data are needed in order to (1) improve solid propellant performance predictive capabilities, (2) provide needed input to current steady-state combustion models which include oxidizer-metal interactions, (3) provide data on the effects of motor and propellant conditions on exhaust signature and (4) provide in-motor particle size distributions which will allow more accurate predictions of damping in stability analyses. The techniques employed have been high speed motion pictures of strand burners and slab burners in a cross-flow environment, SEM analysis of post-fire residue (strand, slab, and motor), determination of changes in  $D_{32}$  across the exhaust nozzle using measurements of scattered laser light, and holograms of burning propellant in strands, slabs, and motors. In addition, considerable effort has been directed toward development of automatic data retrieval methods for obtaining particle size distributions from holograms taken of the combustion of solid propellants. The holographic effort is a two-part problem. Techniques must be developed for obtaining good quality holograms in a realistic solid propellant combustion environment. However, these holograms are of limited value unless the particle size data can be obtained from them in a reasonable time period. This requires development of computer-aided image analysis techniques.

In previous efforts [Refs. 16-19] the motion picture and holographic techniques were successfully demonstrated using propellant strands with up to 15% aluminum. Fourteen micron resolution was obtained in the high speed motion pictures with a 1:12 magnification (and very small depth of field). In addition, initial determinations of  $D_{32}$  were made using measurements of scattered laser light at the entrance and exhaust of a small rocket motor. Apparatus modifications were then made to expand and improve the obtainable data.

The light scattering measurement apparatus developed at NPS can currently be used to determine mean particle sizes ( $D_{32}$ ) at the entrance and exhaust planes of the exhaust nozzle within certain constraints. The present optics limit the measurements to particles larger than approximately three microns. Pressure levels and metal mass loadings also limit the technique to conditions where the transmittance is greater than approximately 20%. Holograms with a resolution limit of approximately four microns and automatic particle size data retrieval from the holograms (with a current resolution limit of approximately 15 microns) can be used to determine particle size distributions at the nozzle entrance where velocities are not excessive. In addition, a Malvern 2600 HSD particle sizer is being used to obtain particle size distributions with a lower size limit of approximately 0.5 microns.

#### DETERMINATION OF PARTICULATE SIZE USING MEASUREMENTS OF SCATTERED LIGHT

##### BACKGROUND

The NPS developed apparatus is based upon diffractively scattered light. The diffraction patterns of light scattered by particles are analyzed to determine the volume-to-surface mean diameter ( $D_{32}$ ). This method has the disadvantages that size distributions cannot be easily determined and particles larger than some threshold size will not be detected due to the exceedingly small angles at which they scatter light. However, it has the advantage that it is non-intrusive and, in theory, can be used in the internal motor environment. Propellant composition can limit the application of the technique by producing large particulates and/or very dense particle clouds.

The completely general theory of scattering was developed by Mie and is presented by Van de Hulst [Ref. 15]. The light scattering characteristics for spherical particles of any size are fully described and the phenomena of reflection, refraction, diffraction and absorption are considered. For particle sizes much smaller than the wavelength of the illuminating light source, the Mie equations simplify to what is called Rayleigh scattering.

The size of the particles of interest in solid propellant rocket motor combustion depends upon the application. Most applications are concerned with particles having diameters much greater than the wavelength of visible light. Scattering by these larger particles is described by Fraunhofer diffraction. Measuring the particle size for a monodispersion can be accomplished by measuring the angular position of a dark or bright ring in the diffraction pattern. This method is not used for polydispersions since the discrete rings are not observed. However, Dobbins, et al. [Ref. 7] found that the volume-to-surface mean diameter of a polydispersion ( $D_{32}$ ) defined by

$$D_{32} = \frac{\int_0^{D_{\max}} N_r(D) D^3 dD}{\int_0^{D_{\max}} N_r(D) D^2 dD} \quad (1)$$

(where  $N_r(D)$  is a distribution function describing the proportion of particles with diameter  $D$  in the sample), could be accurately measured. The value of  $D_{32}$  was shown to be quite insensitive to the form of  $N_r(D)$ . In addition, the ratio of forward scattered light at two forward angles is dominated by Fraunhofer diffraction. The ratio is therefore insensitive to the particle refractive index and

the particle concentration [Ref. 13]. To evaluate the integrated intensity over particle sizes requires specification of  $N_r(D)$ . Dobbins et al. [Ref. 7] used the Upper-Limit-Distribution-Function developed by Hugel and Evans [Ref. 9], and this approach was followed in the present investigation.

For  $\pi D_{32} \theta / \lambda$  (where  $\theta$  is the scattering angle and  $\lambda$  is the wavelength) less than 3.0, a Gaussian curve [Ref. 14] can be used which closely matches the theoretical intensity profile obtained by integrating the Fraunhofer diffraction expression together with the Upper-Limit-Distribution-Function [Ref. 7]. This Gaussian expression has been presented by Buchele [Ref. 14] and is given by

$$I_{\theta} / I_{\theta=0} = \exp - (0.57 \pi D_{32} \theta / \lambda)^2 \quad (2)$$

Equation (2) can be used to obtain the intensity ratio between two (within the apparatus limits) forward scattering angles:

$$I_2 / I_1 = \exp - D_{32}^2 [(\theta_2^2 - \theta_1^2) (0.57 \pi / \lambda)^2] \quad (3)$$

The NPS designed system has been discussed previously [Refs. 18, 19], including calibrations and initial utilization with motor firings. A schematic of the apparatus is shown in Fig. 1. Briefly, it consists of a He-Ne light source, a focusing lens, and a 1024 element linear diode array. Multiple sweeps of the array are made during a motor firing and the averaged intensity vs. scattering angle profile is used to obtain  $D_{32}$  from equation (3). In the present apparatus scattered light can be measured within an angle increment of approximately .05 radians, with a minimum angle of approximately .008 radians. The angle increment is currently being upgraded to .10 radians by using 2048 element linear diode arrays. This will provide more accurate determination of  $D_{32}$  and extend the measureable particle diameter down to approximately 0.5 microns (from the current 2-3 micron range).

A Malvern 2600 Particle Sizer is also being used. The Malvern 2600 uses a 2 mW, He-Ne Laser (632.8 nm wavelength) with a 9 mm diameter, collimated, and spatially filtered beam. The illumination source and detector are mounted on a rigid optical bench. The detector uses three interchangeable Fourier Transform Lens with focal lengths of 63, 100, and 300 mm. Their respective particle sizing ranges are 1.2-118, 1.9-188, and 5.8-564 microns, with a sub-class down to 0.5 microns. When the sub-class is included, the dynamic range is 180:1 on any of the three range settings with an advertised accuracy of +/-4% on volume median diameter. The 100 mm lens with a particle range of 1.9-199 microns was used during this investigation.

The Malvern 2600 detector uses a 31 element solid state array of concentric semicircular diode rings. The 31 rings are sampled in parallel through individual amplifiers. The sample/hold electronic construction uses A/D conversion and on board digital storage. This electronic arrangement provides a sampling time of 10-15 microseconds, overcoming the limitation imposed by a minimum computer read-in time of approximately 25 msec. Output from the Malvern includes both a volume and number distribution, as well as  $D_{32}$ ,  $D_{43}$ , etc.

System control in the manual mode (internal trigger) was provided by operator interface, via the keyboard of the Malvern systems's AT&T 6300PC. The automatic mode (external trigger) was controlled by an HP9836S, simultaneously with the locally designed system. This was incorporated by using a 100 Hz signal generator to provide a 5.0 volt, triangular wave to trigger the Malvern's Spray Synchronizer, which provides triggering control to the Malvern in the external mode. This external trigger signal was supplied via a switching network in the HP9836S computer system.

Data acquisition was accomplished using the Malvern's MASTER-SIZER operating system. This operating system uses a command base language that allows the user to specify the instrument operations and analysis restrictions. The "Model Independent" analysis program is able to measure multimodal particle sizes, and was used exclusively for reduction of Malvern data.

#### MOTOR COMPONENTS

A schematic of the small rocket motor is shown in Fig. 2. Both center-perforated and end-burning grains were used. Two AP/HTPB propellants were used. One contained a small amount of HMX and 1%, 6 micron ZrC. The other contained 2%, 40 micron aluminum.

Currently, a two-dimensional motor is being used which reduces the optical depth through the motor and permits larger scattering angles to be measured.

#### RESULTS AND DISCUSSION

A metal oxide powder containing particles with a nominal size range of 1-20 microns and a mean diameter of 5-8 microns was suspended in distilled water and used as a calibration medium. A glass container measuring approximately 25 mm wide by 20 mm high by 6 mm deep was used to hold the sample, and a glass stirring rod was used to mix the sample during measurements.

At this point of the investigation the equipment was arranged so that the NPS system would make measurements in the nozzle exhaust and the Malvern would make measurements in the internal motor environment. Therefore, when making calibrations using the Malvern, the sample was placed inside the motor cavity with the nitrogen purge filters and the fused silica windows installed. The standard calibration procedure for the NPS system was used. Because of the Malvern's lower tolerance for light obscuration, the sample used with the NPS system was then diluted by a factor of four prior to its measurement with the Malvern 2600.

Figure 3 shows the  $D_{32}$  obtained from the NPS system was 5.5 microns.

Because of the window size used in the motor, the maximum angle that scattered light could pass unobstructed from the motor was approximately  $6^\circ$ . This required the removal of the data received by the Malvern's outer three rings using a "KILLDATA 0,3" command in the Master Sizer mode. This limited the Malvern's measureable particle range to a minimum of 3.5 microns vice the 1.9 microns normally expected when using the 100 mm focal lens. Figure 4 shows the tabulated volume distribution and the associated distribution graph, which indicated a  $D_{32}$  of 5.8 microns. The Malvern and NPS values for  $D_{32}$  agreed within 5.5%.

Prior to the final two rocket firings the two light scattering apparatuses were switched so that the NPS system would measure in the internal motor environment and the Malvern would measure in the nozzle exhaust. A calibration was conducted on the NPS system using the same procedures and equipment as before, with the exceptions that 9.6 micron polystyrene spheres were used and the sample was measured while sitting in the motor cavity with the nitrogen purge filters and fused silica windows installed. The  $D_{32}$  calculated by the NPS system was 9.6 microns (Fig. 5).

Results from the firings are presented in Table I.

Test No.	Wt. of Metal (%)	Meas. Press (psig)	Burn Time (sec)	Motor $D_{32}$ (microns)	Exhaust $D_{32}$ (microns)
1	1.0 ZrC	124	7.2	43.0(V) 27.0(N)	9.5 (NPS) (?)
2	1.0 ZrC	119	6.5	47.7(V) 32.4(N)	6.5 (NPS) (?)
3	1.0 ZrC	175	~ 5	24-25 (NPS)	127(V) 127(N)
4	1.0 ZrC	125	~ 6.5	29 (NPS)	127(V) 127(N)
5	2.0 Al	265	3.5	4.3(V) 4.3(N)	6.2 (NPS)
6	2.0 Al	238	3.4	4.3(V) 4.3(N)	4.6 (NPS)
7	2.0 Al	233	2.9	4.4 (NPS)	127.1(V) 122.6(N)
8	2.0 Al	211	3.8	4.6 (NPS)	97.6(V)

(V) - - Malvern Volume Distribution  $D_{32}$   
 (N) - - Malvern Number Distribution  $D_{32}$   
 (NPS) - NPS System

Tests 1-4 were made using the ZrC propellant. The measured  $D_{32}$ 's in the exhaust using the NPS system were 6.5 and 9.5 microns. The data may have been biased slightly (1-2 microns) high due to several bad diodes in the array (which affected the averaging procedure). When the Malvern system

was used in the exhaust region  $D_{32}$  was 127 microns. The NPS system (with the current optical arrangement) could not accurately detect particles larger than approximately 30 microns. This discrepancy is discussed below.

In the motor cavity the  $D_{32}$  values from the Malvern number distributions and the NPS system were in good agreement (24-32 microns). Typical results from sampling the internal motor environment with the Malvern are shown in Fig. 6 and 7. The measured  $D_{32}$ 's in the motor indicated that significant agglomeration of the 6 micron zirconium-carbide particles in the burning propellant occurred. However, residual inhibitor could also bias the results. This is one example of why both holography and measurements of scattered light should both be used when possible. It is more difficult to obtain the particle size distribution from holograms and the minimum detectable particle size is limited to several microns. However, the presence of larger material, other than spherical particles, are readily observed.

A sample of the Test 1 post-fire residue was removed from the motor cavity in the vicinity of the windows (Fig. 8) and from the converging section of the graphite nozzle (Fig. 9 and 10). These samples were multiple-washed using acetone and then examined using an electron microscope (SEM). The observed spherical particle sizes in the small sample ranged from 1-20 microns. These were somewhat smaller than would be indicated by a  $D_{32}$  between 27.0 and 47.7 microns as measured by the Malvern. The SEM did indicate the presence of larger irregular shaped particles, but their source/composition could not be determined.

The pressure time traces for both Tests 1 and 2 indicated a series of random short pressure spikes. During Test 1 a KODAK Ektapro high speed video camera recorder (VCR) was used to monitor the nozzle exhaust plume. The pictures showed periodic expulsion of large agglomerates in conjunction with the pressure spikes. Particles were apparently agglomerating on the converging wall of the nozzle and periodically expelled. This was the apparent reason for the large particles measured by the Malvern.

Tests 5-8 were conducted using the 2.0% aluminized propellant. The light scattering measurements were taken on the pressure plateau at 92% and 97% of maximum chamber pressure, with burn times ranging from 2.9 to 3.8 seconds.

In Test 5, the  $D_{32}$  measured by the NPS system at the nozzle exhaust was approximately 6.2 microns. In Test 6, the NPS system measured a  $D_{32}$  of 4.6 microns. For the same tests, the Malvern measured internal motor environment  $D_{32}$ 's of 4.3 microns (Figures 11 and 12) based on both volume and number.

A sample of the Test 5 post-fire residue was removed from the converging section of the graphite nozzle. SEM photographs of the residue displayed spherical particle sizes ranging from less than 1.0 to greater than 30 microns. Large irregular shaped particles similar to those viewed in the Test 1 samples were also present in large numbers.

The Malvern and NPS systems were then switched so that the NPS system would measure the internal motor environment and the Malvern would measure in the nozzle exhaust. The calibration of the NPS system was verified using 9.6 micron particles as discussed earlier.

Since the maximum scattering angle of the Malvern was no longer limited by the rocket motor window, no rings of data were deleted from the analysis. The Tests 7 and 8 nozzle exhaust volume distribution  $D_{32}$  measurements made with the Malvern were 127.1 and 97.6 microns respectively. The number distribution  $D_{32}$  measurement in Test 7 was 122.6. The Test 8 results indicated a tri-modal volume distribution of particles (Figure 13).

The Tests 7 and 8 internal motor environment  $D_{32}$ 's measured by the NPS system (Figure 14) were 4.4 and 4.6 microns.

During these four tests the  $D_{32}$  values obtained for the motor environment from both the Malvern and NPS systems were in excellent agreement (within 7%). The  $D_{32}$  values obtained in the exhaust using the NPS system were consistent, but the system was not capable of measuring the very large particles observed by the Malvern.

#### AUTOMATIC DATA RETRIEVAL FROM ROCKET MOTOR HOLOGRAMS

#### BACKGROUND

Holographic techniques have been employed to capture the dynamics of the combustion chambers of small rocket motors while firing. These techniques are being refined and upgraded. Concurrently, improvements in the processing of the holograms to extract the particle size distributions are also necessary.

Once the hologram has been successfully recorded, it is desirable to have a computer process the image to measure the particle size and to produce a statistical description of the particle size distribution. The steps required to produce this distribution follow.

1. Image acquisition from the hologram reconstruction,
2. Image digitization and storage on the computer system,
3. Speckle reduction filtering to separate the particle image information from the overlaying speckle,
4. Application of an image threshold to separate the image features from the background features,
5. Feature identification to find the connected feature pixels and "recognize" the connected pixels as a single object,
6. Feature sizing to measure the number of features, the area, x-chord width, y-chord width, particle roundness, and centroid location, and
7. Histogram production using the size data of the prior step.

The acquisition and digitization of the image along with preliminary processing and sizing techniques have been described in earlier papers [Refs. 19-20]. The process is done with a commercial image processing board in a PC/AT microcomputer. Commercial image processing subroutines are mixed with locally produced programs to perform the desired image processing and measurements. Recently, an upgraded processor board with a 386 microprocessor has been added to the computer system to speed up processing.

#### TEST OBJECTS

Three test objects have been used in our investigations. These objects were imaged under white light as the highest contrast images with the most benign background. These images provide a resolution calibration. The objects were also recorded in holograms in the test setup to duplicate the test geometry.

The first object was a calibration reticle produced by LEOS, Inc. The circular portion of the reticle consisted of approximately 10,000 opaque circular features of twenty-three sizes, ranging from five to ninety-three micrometers in diameter. These circles are photodeposited in an eight millimeter circular area. An array to the right of the circular test pattern consists of the twenty-three standard sizes.

The second object was the 1951 USAF Standard Resolution chart. This was used for resolution studies as it provides a more continuous measurement of resolution degradation than the Calibration array.

The final object was the reconstruction from rocket motor holograms recorded during firing using propellant samples supplied by the Air Force.

#### SIZING INVESTIGATIONS

The processing of the digitized image proceeds as follows:

- o Image averaging to partially reduce speckle. The real image of the reconstructed hologram is focused on a spinning mylar disk. The disk motion temporally varies the speckle pattern while the particle images remain stationary. The integration time of the vidicon causes the speckle to be reduced by averaging.
- o The speckle was further reduced through various processing algorithms. An investigation into the tradeoff between resolution and speckle reduction are discussed below.
- o The next processing step is the application of a threshold to remove all information from the background. Figure 15 shows a comparison illustrating the filtering effect. Figure 15a is a thresholded image after the image was averaged but not filtered before applying the threshold. Significant error due to the speckle effects is present. Figure 15b shows the same image, but with the speckle reduction filter applied before applying the threshold. Far less noise is present.
- o The thresholded image was then processed by the Fortran routine for object identification, counting, and sizing. The object identification is done by scanning the data array for adjacent pixels (currently in the horizontal and vertical directions only, with no check made on diagonals). Adjacent pixels are joined to form one object or "feature." The area and maximum chord widths are then computed for each object and written into a data table. (If desired, a roundness test can be applied to the chord length measurements to eliminate non-spherical particles.) This data table is processed to produce the final histogram data on particle size.

Significant effort was spent to improve the speed and efficiency of these programs. Early efforts were limited to a 256 x 256 picture due to processing times (on the order of 4 hours) and memory constraints. Now 512 x 512 images can be handled in approximately 10 minutes from frame digitization to production of the data table. Improvements have been due to commercial availability of software that manipulates the fast-access video memory board, improved software revisions on locally produced programs, and the addition of a faster microprocessor. Further reductions in time can be made by using more powerful and more expensive computer hosts for the image processing board. The time currently required is appropriate for the feasibility studies that we are carrying out.

#### MEASUREMENT RESULTS

Figure 16 shows a frequency histogram of particle size distribution as measured from an experimental hologram taken during a rocket firing. The horizontal axis is the x-width of the particle. The data represents 1,592 particles that were obtained by combining the data from 16 different regions in the hologram reconstruction.

The field of view of the microscope system is determined by the magnification required to resolve the smallest particle. The number of particles within the field of view depends on the size of the field of view. For the small fields of view required for small particles the number of views to completely cover a hologram can approach the millions. One question of interest, then, was how many particles were enough to provide a meaningful set of statistics. Figure 17 represents the data from 96 particles in one field of view. Figure 18 is the data from 681 particles in seven fields of view. Figure 19 represents the data from 984 particles in ten fields of view; it has the general shape of the distributions from larger numbers of particles for this hologram. For this hologram we have experimentally concluded that approximately 1,000 particles need to be measured before the distribution stays about the same. Further experimentation is necessary to establish confidence levels in the data for this image and to see if the results vary widely between images.

#### SPECKLE REDUCTION STUDIES

Speckle reduction techniques that use simple convolution techniques were described in Ref. 19. More involved speckle reduction filters [Refs. 22,23,24] that reduce the speckle, but attempt to preserve the edges of the objects, were also described in Ref. 19. Figure 20 shows the reduction in speckle (as measured quantitatively by the speckle index) versus the number of iterations of the speckle reduction filter. The filters shown are three nonlinear filters taken from the synthetic aperture community (the local statistics filter, the sigma filter, and the geometric filter) and two locally developed filters (the 5 x 5 convolution filter, and the 3 x 3 gaussian filter). While all but the 3 x 3 gaussian filters were approximately equally successful in reducing the speckle after four or more iterations, the question arose about the magnitude of the resolution degradation that accompanies speckle reduction. To measure speckle reduction, holograms were made of the 1951 Air Force Resolution chart (Fig. 21). The resolution could be measured after each iteration of the speckle reduction filter. Figure 22 shows the measured resolution of the nonlinear speckle reduction filters. The comparable resolutions for the convolution and gaussian filters are currently being measured but it is expected that the resolution degradation of these filters will be worse since these techniques are known to suffer from significant resolution reduction. (The latter filters are about one order of magnitude faster than the more complicated filters; hence, the user will have to tradeoff speed against resolution reduction. For most applications the faster filters have been used.)

#### CONCLUSIONS

The results of this investigation have shown that the measurements of particle size distributions and  $D_{32}$  can be made through both the exhaust jet and the motor cavity of a small solid propellant rocket motor. To date, the exhaust measurements have been of limited value due to surface agglomeration on, and shedding from, the converging nozzle wall of the small motor.

Holograms have been successfully obtained in the motor environment at low pressures. Two-dimensional motors, which reduce the optical path length through the particles, are currently being used to extend the operating pressure to higher values.

The capability to automatically record the size and location of particles in a hologram reconstruction has been demonstrated. It requires approximately 10 minutes to process an image frame with about 100 particles present on an IBM PC/AT with a 16 MHz 386 microprocessor. Higher processing rates can be achieved with faster computers. Summing the data from independent views of the reconstruction studied suggests that the histogram of the particle size distribution reaches a representative shape after summing information from approximately 1,000 particles. Further study is needed to verify this initial observation.

#### REFERENCES

1. George, D., Recent Advances in Solid Rocket Motor Performance Prediction Capability, AIAA Paper No. AIAA-81-033, 19th Aerospace Sciences Meeting, Jan 12-15, 1981.
2. Hermsen, R.W., Aluminum Oxide Particle Size for Solid Rocket Motor Performance Prediction, AIAA 19th Aerospace Sciences Meeting, Jan 12-15, 1981.
3. Dobbins, R.A., "Remote Size Measurements of Particle Product of Heterogeneous Combustion," Eleventh Symposium (International) on Combustion, The Combustion Institute, 1967, p. 921.
4. Dobbins, R.A. and Strand, L.D., "A Comparison of Two Methods of Measuring Particle Size of  $Al_2O_3$  Produced by a Small Rocket Motor," AIAA J. Vol. 8, pp. 1544-1550, 1970.
5. Cashdollar, K.L., Lee, C.K. and Singer, J.M., "Three Wavelength Light Transmission Technique to Measure Smoke Particle Size and Concentration," Applied Optics, Vol. 18, No. 11, pp. 1763-1769, June 1979.
6. Gumprecht, R.O. and Slipecevic, C.M., "Scattering of Light by Large Spherical Particles," J. Physical Chem., Vol. 57, pp. 90-94, Jan 1953.
7. Dobbins, R.A., Crocco, L. and Glassman, I., "Measurement of Mean Particle Size of Sprays from Diffractively Scattered Light," AIAA J. Vol. 1, No. 8, pp. 1882-1886, 1963.
8. Roberts, J.H. and Webb, M.J., "Measurements of Droplet Size for Wide Range Particle Distributions," AIAA J., Vol. 2, No. 3, pp. 583-585, 1964.
9. Mugele, R.A. and Evans, H.D., "Droplet Size Distribution in Sprays," Ind. and Eng. Chem., Vol. 43, pp. 1317-1324, 1951.
10. Dobbins, R.A. and Jizmagian, G.S., "Optical Scattering Cross-Sections for Polydispersions of Dielectric Spheres," J. Optical Soc. of Am., Vol. 56, No. 10, pp. 1345-1350, 1966.
11. Dobbins, R.A. and Jizmagian, G.S., "Particle Measurement Based on Use of Mean Scattering Cross-Sections," J. Optical Soc of Am., Vl. 56, No. 10, pp. 1351-1354, 1966.
12. Hodkinson, J.R., "Particle Sizing by Means of the Forward Scattering Lobe," Applied Optics, Vol. 5, pp. 839-844, 1966.
13. Powell, E.A., Cassanova, R.A., Bankston, C.P. and Zinn, B., Combustion Generated Smoke Diagnostics by Means of Optical Measurement Techniques, AIAA Paper No. 76-67, AIAA 14th Aerospace Sciences Meeting, Jan. 1976.
14. Buchele, D.R., Particle Sizing by Measurement of Forward Scattered Light at Two Angles, NASA TP 2156, May 1983.
15. Van de Hulst, H. C., Light Scattering by Small Particles, John Wiley and Sons, Inc., New York, 1957.
16. Karagounis, S.G. et al., An Investigation of Experimental Technique for Obtaining Particulate Behavior in Metallized Solid Propellant Combustion, AFRPL-TR-82-051, Air Force Rocket Propulsion Laboratory Report, Edwards AFB, July 1982.
17. Cramer, R.G. et al., An Investigation of Experimental Techniques for Obtaining Particulate Behavior in Metallized Solid Propellant Combustion, AFRPL-TR-84-014, Air Force Rocket Propulsion Laboratory, Edwards AFB, CA, Feb. 1984.
18. Netzer, D.W. and Powers, J.P., Experimental Techniques for Obtaining Particle Behavior in Solid Propellant Combustion, AGARD-CP-391, No. 19, AGARD Conference on Smokeless Propellants, Florence, Italy, 12-13 Sept. 1985.
19. Edwards, T., Horton, K.G., Redman, D., Rosa, J.S., Rubin, J.B., Yoon, S.C., Powers, J.P., Netzer, D.W., Measurements of Particulates in Solid Propellant Rocket Motors, Proceedings of the 21st JANNAF Combustion Meeting, Chemical Propulsion Information Agency, Johns Hopkins University, Laurel, Maryland, pp. 119-132, 1986.
20. Edwards, T.D., Harris, R.K., Horton, K.G., Keith, M.G., Kertadidjaja, A., Redman, D.N., Rosa, J.S., Yoon, S.C., Netzer, D.W. and Powers, J.P., "Measurements of Particulates in Solid Combustion Rocket Motors," To be published as an Air Force Astronautics Laboratory Technical Report, Edwards AFB, CA.

21. Redman, D. N., Image Analysis of Solid Propellant Combustion Holograms Using an Image-Action Software Package, M.S. Thesis, Naval Postgraduate School, Monterey, California, June 1986.
22. Crimmins, T. R., "Geometric Filter for Speckle Reduction," *Optical Engineering*, Vol. 25, No. 5, May 1986.
23. Crimmins, T. R., "Geometric Filter for Speckle Reduction," *Applied Optics*, Vol. 24, No. 10, May 1985.
24. Lee, J. S., "Speckle Suppression and Analysis for Synthetic Aperture Radar," *Optical Engineering*, Vol. 25, No. 5, May 1986.

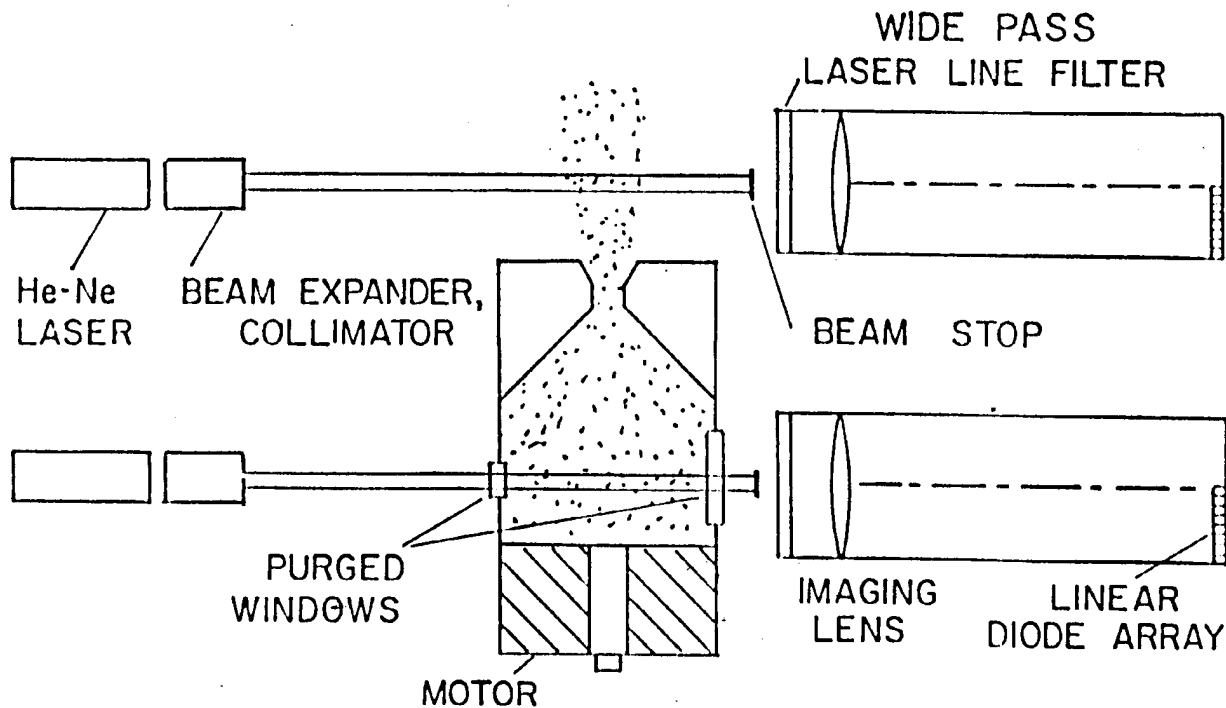


Figure 1. Schematic of Scattered Light Measurement Apparatus

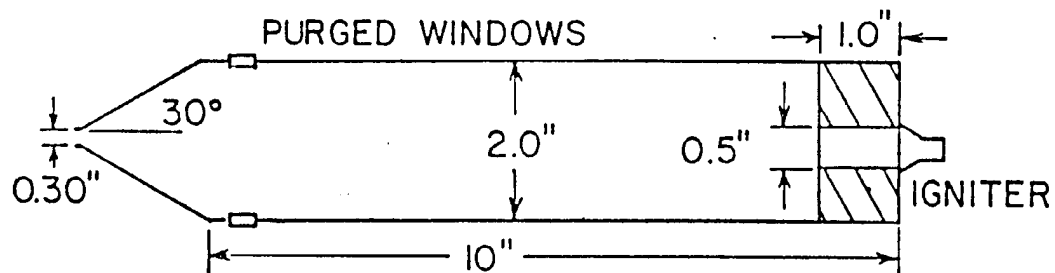


Figure 2. Schematic of Small Solid Propellant Motor

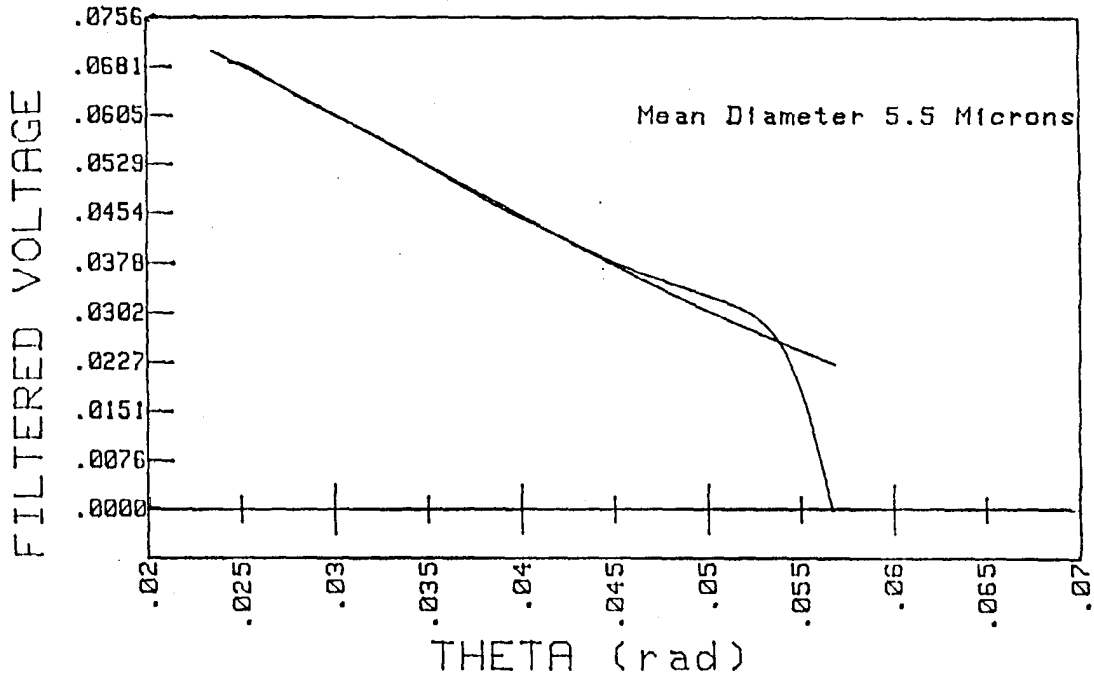
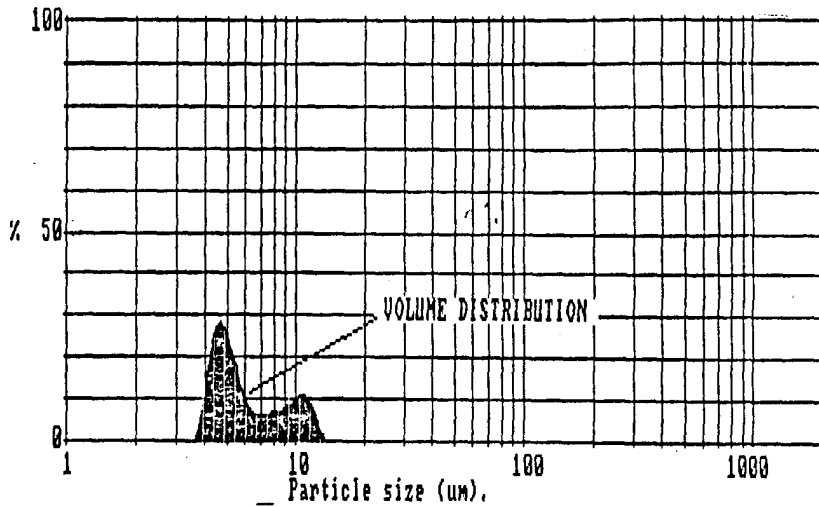


Figure 3. NPS Scattering Measurement Apparatus Calibration, 1-20 Micron Metal Oxide Particles



Size microns	under	% in band	Size microns	under	% in band	Result source=testdata
188.0	100.0	0.0	17.7	100.0	0.0	Record No. = 1
162.0	100.0	0.0	15.3	100.0	0.0	Focal length = 100 mm.
140.0	100.0	0.0	13.2	100.0	5.4	Experiment type pil
121.0	100.0	0.0	11.4	94.5	10.9	Volume distribution
104.0	100.0	0.0	9.8	83.6	7.9	Beam length = 6.0 mm.
89.9	100.0	0.0	8.5	75.7	6.4	Obscuration = 0.5285
77.5	100.0	0.0	7.3	69.3	6.2	Volume Conc. = 0.0244 %
66.9	100.0	0.0	6.3	63.1	11.7	Log. Diff. = 3.15
57.7	100.0	0.0	5.4	51.4	23.9	Model indp
49.8	100.0	0.0	4.7	27.6	24.6	D(v,0.5) = 5.4 μm
42.9	100.0	0.0	4.1	3.0	3.0	D(v,0.9) = 10.7 μm
37.1	100.0	0.0	3.5	0.0	0.0	D(v,0.1) = 4.3 μm
32.0	100.0	0.0	3.0	0.0	0.0	D(4,3) = 6.5 μm
27.6	100.0	0.0	2.6	0.0	0.0	D(3,2) = 5.8 μm
23.8	100.0	0.0	2.2	0.0	0.0	Span = 1.2
20.5	100.0	0.0	1.9	0.0	0.0	Spec. surf. area
						0.70 sq. m./cc.

Figure 4. Malvern Calibration, 1-20 Micron Metal Oxide Particles

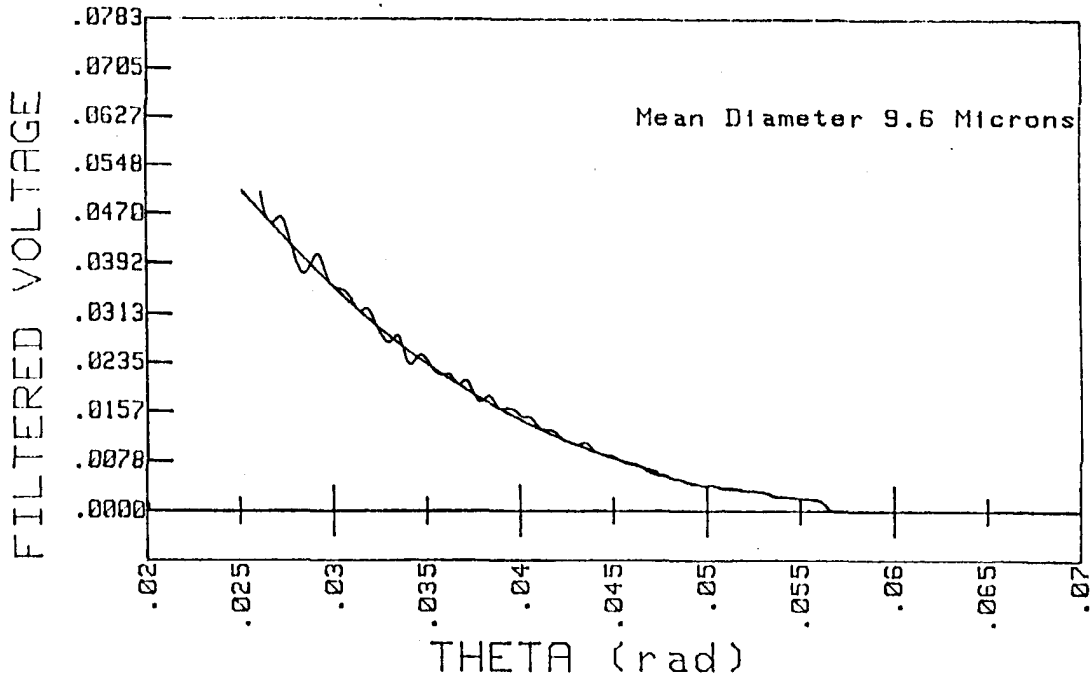
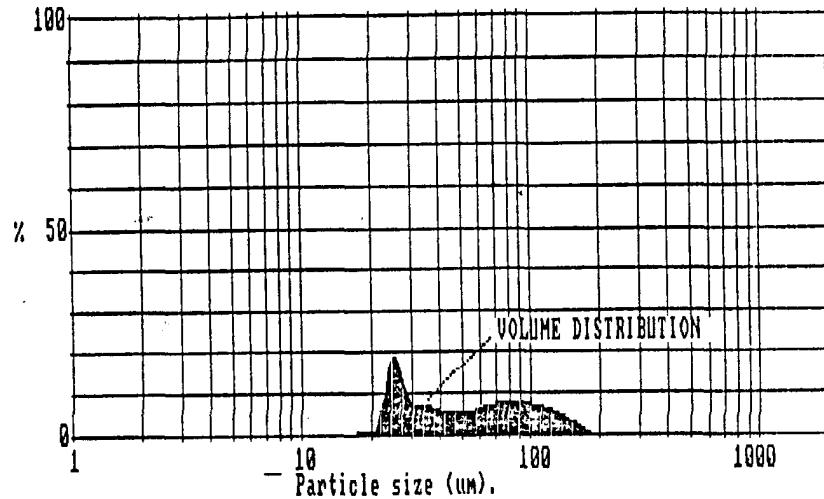
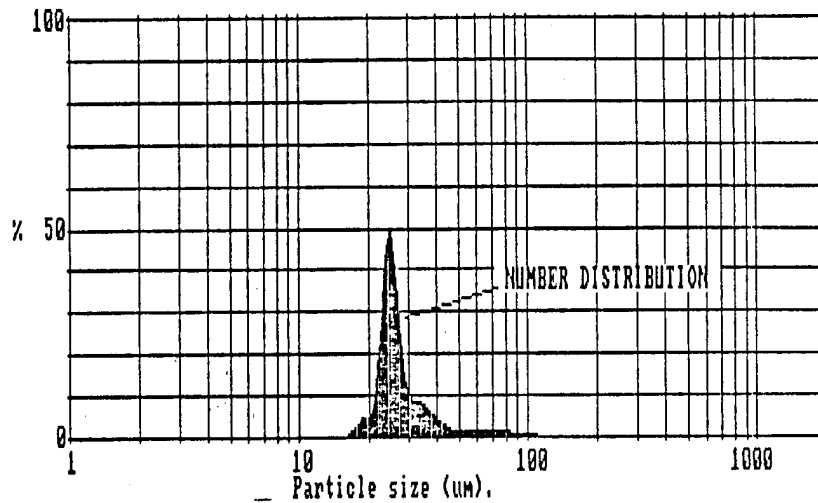


Figure 5. NPS Scattering Apparatus Calibration, 9.6 Micron Polystyrene Spheres



Size microns	under	% in band	Size microns	under	% in band	Result source
188.0	100.0	1.3	17.7	0.2	0.2	testdata
162.0	98.7	3.4	15.3	0.0	0.0	Record No. = 8
140.0	95.4	5.1	13.2	0.0	0.0	Focal length = 100 mm.
121.0	90.3	6.6	11.4	0.0	0.0	Experiment type pia
104.0	83.8	7.1	9.8	0.0	0.0	Volume distribution
89.9	76.6	7.6	8.5	0.0	0.0	Beam length = 51.0 mm.
77.5	69.1	7.3	7.3	0.0	0.0	Obscuration = 0.9864
66.9	61.8	6.5	6.3	0.0	0.0	Volume Conc. = 0.1236 %
57.7	55.3	5.2	5.4	0.0	0.0	Log. Diff. = 6.10
49.8	50.0	5.0	4.7	0.0	0.0	Model indep
42.9	45.1	5.6	4.1	0.0	0.0	D(v, 0.5) = 49.8 μm
37.1	39.5	6.9	3.5	0.0	0.0	D(v, 0.9) = 120.1 μm
32.0	32.6	7.2	3.0	0.0	0.0	D(v, 0.1) = 24.3 μm
27.6	25.4	18.0	2.6	0.0	0.0	D(4, 3) = 61.8 μm
23.8	7.3	6.3	2.2	0.0	0.0	D(3, 2) = 43.0 μm
20.5	1.0	0.8	1.9	0.0	0.0	Span = 1.9
						Spec. surf. area
						0.06 sq. m./cc.

Figure 6. Malvern Volume Distribution Results, Test 1, Motor Cavity, ZrC



Size microns	under	% in band	Size microns	under	% in band	Result source=testdata
188.0	100.0	0.0	17.7	1.0	1.0	Record No. = 8
162.0	100.0	0.0	15.3	0.0	0.0	Focal length = 100 mm.
140.0	100.0	0.1	13.2	0.0	0.0	Experiment type pia
121.0	99.9	0.4	11.4	0.0	0.0	Number distribution
104.0	99.5	0.7	9.8	0.0	0.0	Beam length = 51.0 mm.
89.9	98.8	1.1	8.5	0.0	0.0	Obscuration = 0.9864
77.5	97.7	1.4	7.3	0.0	0.0	Volume Conc. = 0.1236 %
66.9	96.3	1.4	6.3	0.0	0.0	Log. Diff. = 6.10
57.7	94.9	1.3	5.4	0.0	0.0	Model indp
49.8	93.6	1.9	4.7	0.0	0.0	D(v,0.5) = 25.6 μm
42.9	91.7	4.4	4.1	0.0	0.0	D(v,0.9) = 40.0 μm
37.1	87.3	7.8	3.5	0.0	0.0	D(v,0.1) = 22.4 μm
32.0	79.5	9.6	3.0	0.0	0.0	D(4,3) = 29.9 μm
27.6	69.9	45.4	2.6	0.0	0.0	D(3,2) = 27.0 μm
23.8	24.5	19.0	2.2	0.0	0.0	Span = 0.7
20.5	5.5	4.5	1.9	0.0	0.0	Spec. surf. area
						0.06 sq.m./cc.

Figure 7. Malvern Number Distribution Results, Test 1, Motor Cavity, ZrC

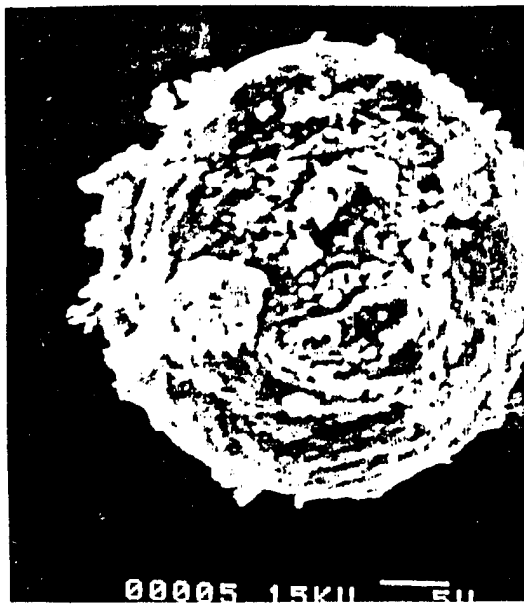


Figure 8. SEM Photograph, Combustion Products From Wall Near Windows, Test 1, ZrC

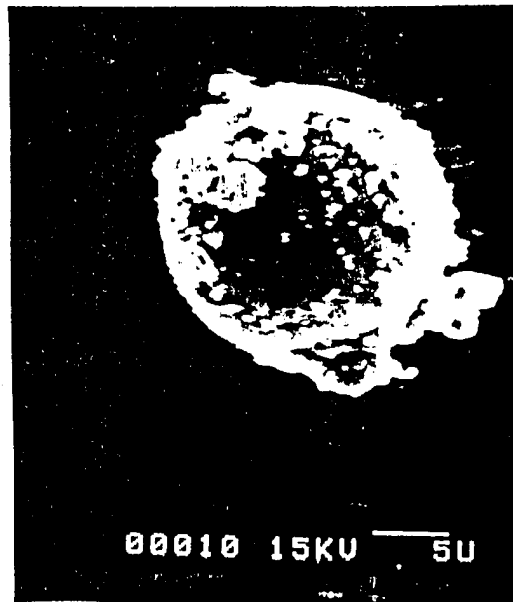


Figure 9. SEM Photograph, Combustion Products From Converging Nozzle Wall, Test 1, ZrC

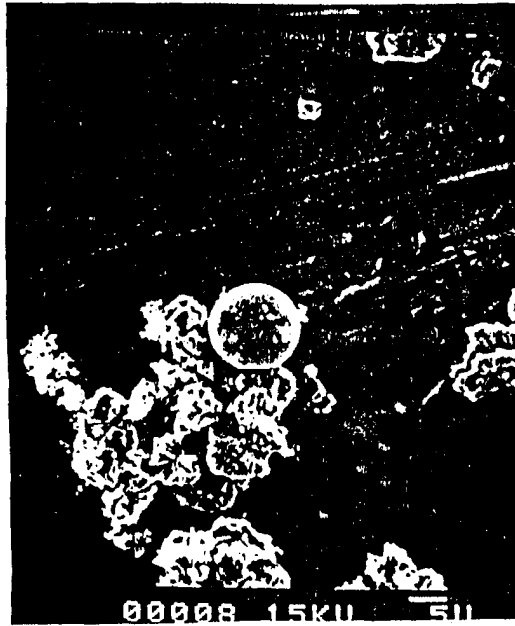
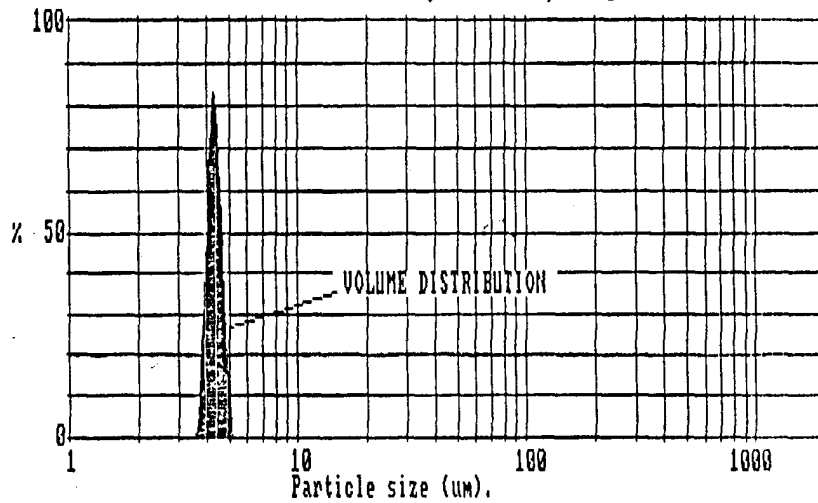


Figure 10. SEM Photograph, Combustion Products From Converging Nozzle Wall, Test 1, ZrC



Size microns	under	% in band	Size microns	under	% in band	Result source=testdata
188.0	100.0	0.0	17.7	100.0	0.0	Record No. = 13
162.0	100.0	0.0	15.3	100.0	0.0	Focal length = 100 mm.
140.0	100.0	0.0	13.2	100.0	0.0	Experiment type pia
121.0	100.0	0.0	11.4	100.0	0.0	Volume distribution
104.0	100.0	0.0	9.8	100.0	0.0	Beam length = 51.0 mm.
89.9	100.0	0.0	8.5	100.0	0.0	Obscuration = 0.0407
77.5	100.0	0.0	7.3	100.0	0.0	Volume Conc. = 0.0001 %
66.9	100.0	0.0	6.3	100.0	0.0	Log. Diff. = 6.62
57.7	100.0	0.0	5.4	100.0	5.0	Model indep
49.8	100.0	0.0	4.7	94.9	80.3	D(v,0.5) = 4.3 μm
42.9	100.0	0.0	4.1	14.6	14.6	D(v,0.9) = 4.6 μm
37.1	100.0	0.0	3.5	0.0	0.0	D(v,0.1) = 4.0 μm
32.0	100.0	0.0	3.0	0.0	0.0	D(4,3) = 4.3 μm
27.6	100.0	0.0	2.6	0.0	0.0	D(3,2) = 4.3 μm
23.8	100.0	0.0	2.2	0.0	0.0	Span = 0.1
20.5	100.0	0.0	1.9	0.0	0.0	Spec. surf. area
						1.40 sq. m./cc.

Figure 11. Malvern Volume Distribution Results, Test 5, Motor Cavity, Aluminum

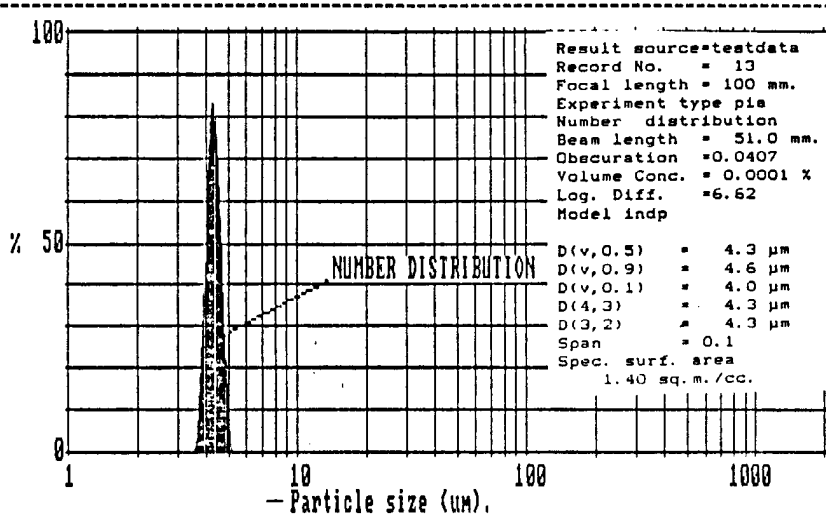


Figure 12. Malvern Number Distribution Results, Test 5, Motor Cavity, Aluminum

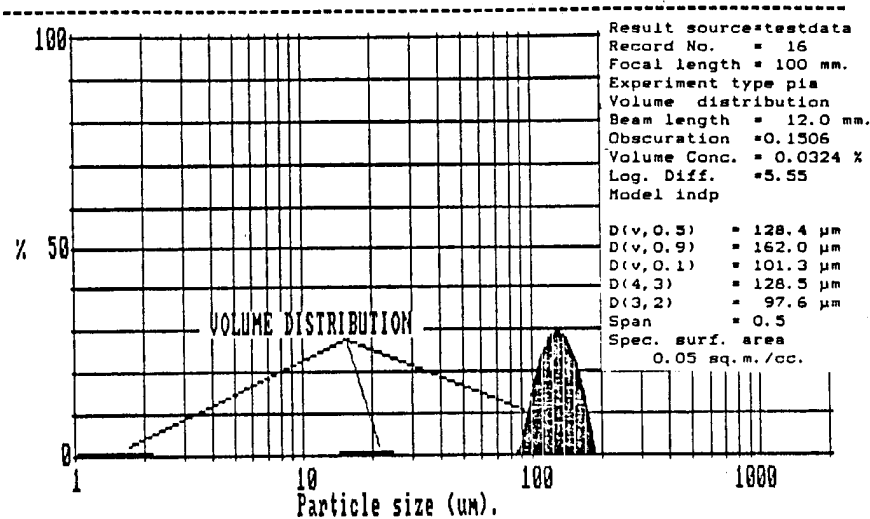


Figure 13. Malvern Volume Distribution Results, Test 8, Exhaust, Aluminum

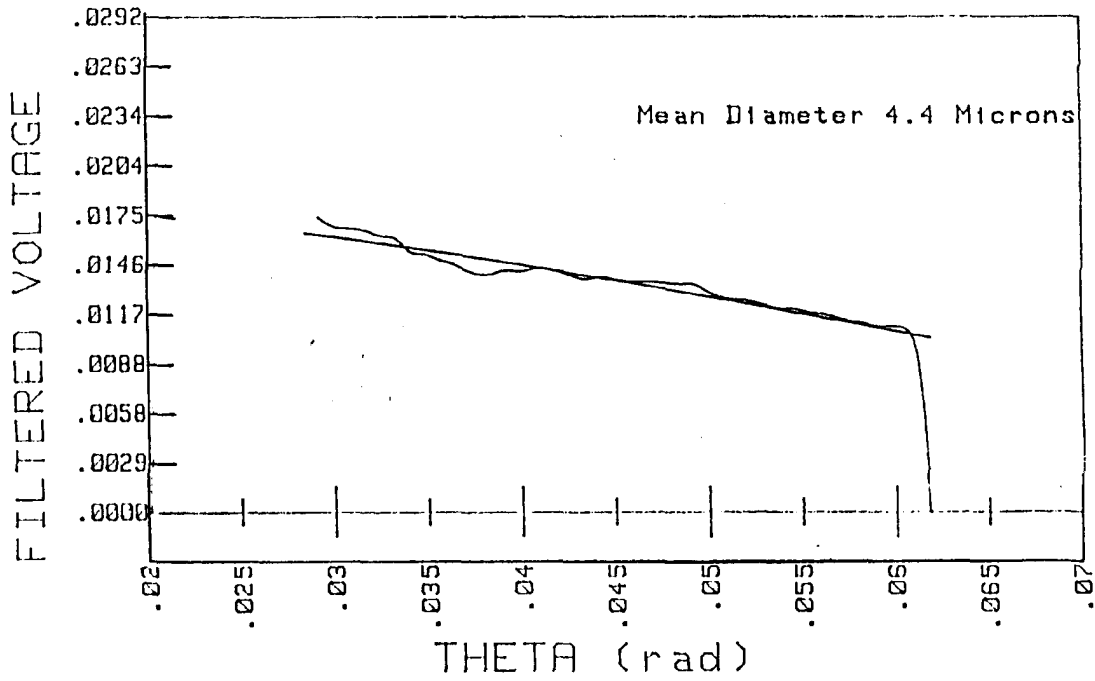
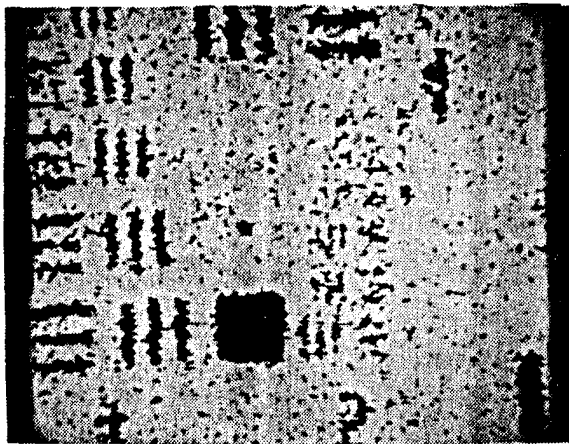
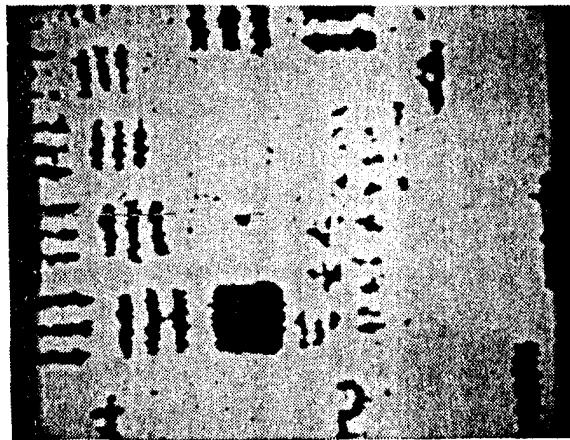


Figure 14. NPS Apparatus Results, Test 7, Motor Cavity, Aluminum



(a)



(b)

Figure 15. Effects of filtering on processed images: (a) Averaged and threshold applied (no speckle reduction filter), (b) Averaged, speckle-reduction filtered, and threshold applied

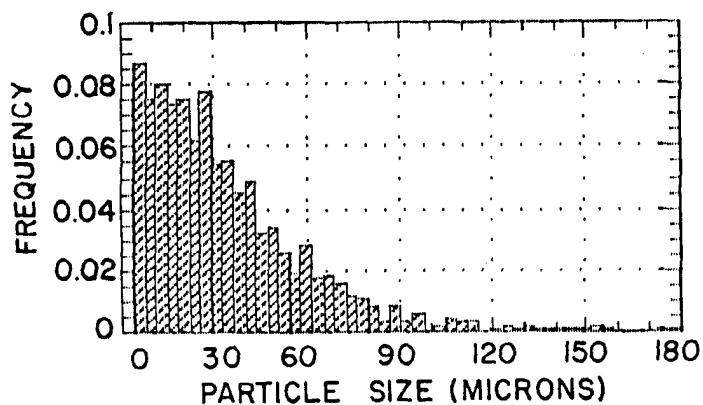


Figure 16. Histogram of particle sizes (in microns) for 1,592 particles contained in 16 fields of view.

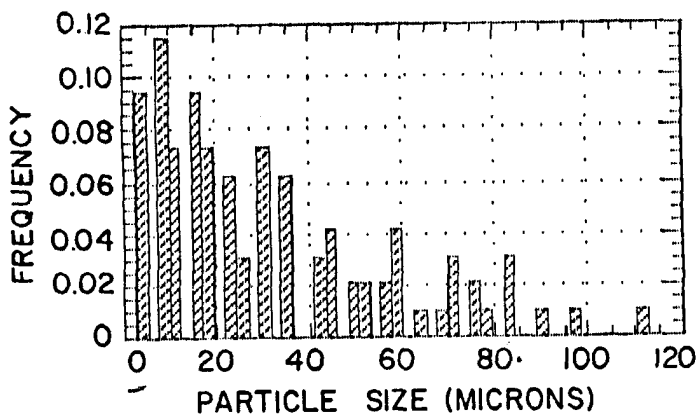


Figure 17. Histogram of particle sizes (in microns) for 96 particles contained in one field of view.

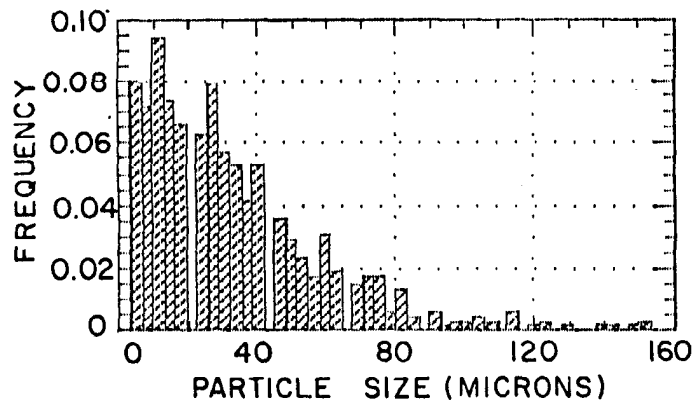


Figure 18. Histogram of particle sizes (in microns) for 681 particles contained in 7 fields of view.

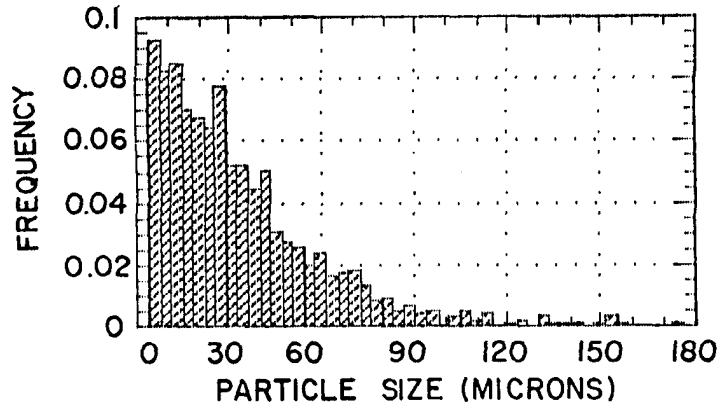


Figure 19. Histogram of particle sizes (in microns) for 984 particles contained in ten fields of view.

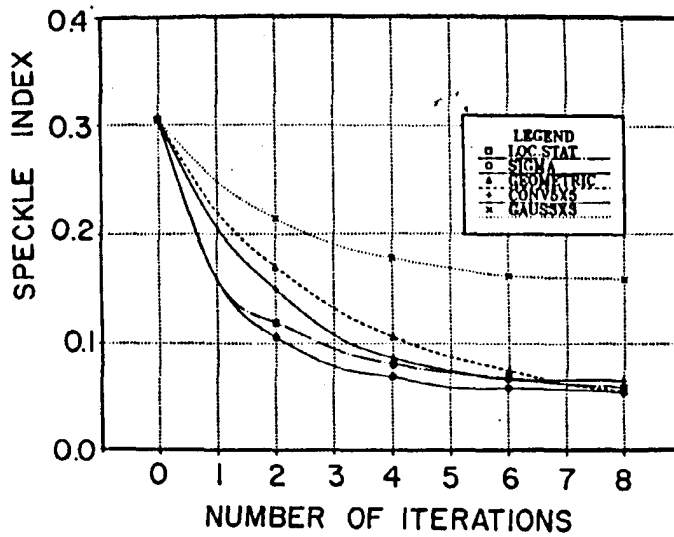


Figure 20. Reduction in speckle level (Speckle Index) vs. number of iterations of speckle filter for five different speckle reduction filters.

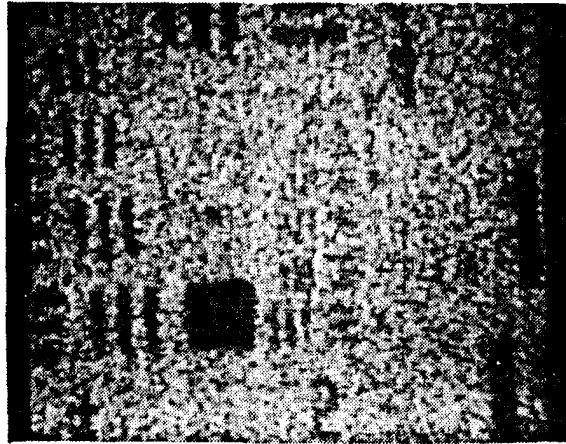


Figure 21. Sample hologram reconstruction of AF resolution chart (before speckle reduction).

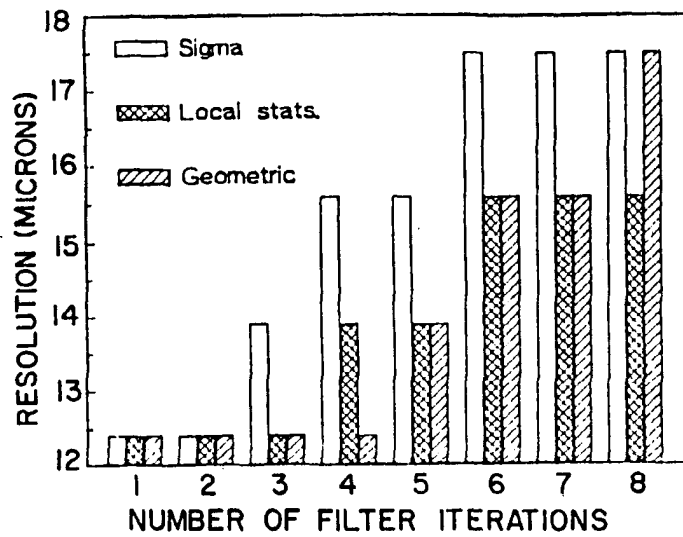


Figure 22. Measured resolution vs. number of iterations of speckle reduction filter for three reduction filters.